JOC Article

Medium Effect on the Rotational Barrier of Carbamates and Its Sulfur Congeners

Rodrigo M. Pontes, Ernani A. Basso,* and Francisco P. dos Santos

Departamento de Química, Universidade Estadual de Maringá, Av. Colombo, 5790, 87020-900 Maringá-PR, Brazil

eabasso@uem.br

Received September 19, 2006

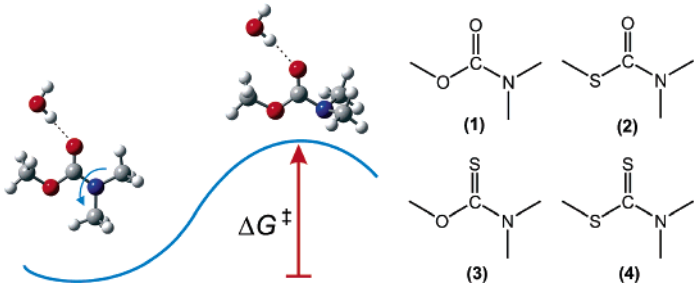

The solvent effect on rotation about the conjugated C−N bond has been studied for methyl *N*,*N*-dimethylcarbamate (**1**), *S*-methyl *N*,*N*-dimethylthiocarbamate (**2**), *O*-methyl *N*,*N*-dimethylthiocarbamate (**3**), and methyl *N*,*N*-dimethyldithiocarbamate (**4**). The present investigation included experimental determination of activation parameters ($\Delta H^{\ddagger}$, $\Delta S^{\ddagger}$, and $\Delta G^{\ddagger}$) combined with theoretical calculations via both quantum and classical approaches. Rotational barriers were measured through dynamic NMR experiments in solvents of varied polarity and proton donor ability. In the less polar solvents, the values were 15.3 ± 0.5 (CS_2), 14.0 ± 1.1 (CS_2), 17.5 ± 0.4 (CCl_4), and 14.6 ± 0.5 kcal/mol (CCl_4) for **1**, **2**, **3**, and **4**, respectively. Upon changing to an aqueous solution, the greatest variations occurred for **2** and **4**, whereas for **1** and **3**, there was no observable effect. Quantum chemical calculations at the HF/6-311+G(2d,p) and B3LYP/6-311+G(2d,p) levels, with the inclusion of solvation effects via the isodensity polarizable continuum model (IPCM), correctly reproduced the experimentally observed trends but failed to account for some of the measured rotational barrier's magnitudes. Hydrogen-bonding effects were included by performing molecular dynamic simulations. For these latter calculations, it was necessary to parametrize the force field against energies of water−solute complexes calculated at B3LYP/6-31+G-(d,p). Through the results of radial distribution functions, solution rotational barriers could be calculated, presenting good agreement with experimental determinations and revealing the role of hydrogen bonding. Interestingly, only for **2**, the rotational barrier is predicted to increase as a result of complexation with water. For the remaining compounds, hydrogen bonding causes the barrier to decrease, contrasting with most of the molecular systems studied up to now.

Introduction

When a nitrogen atom is attached to a double bond (as in >N−C═O), its lone pair can delocalize over the π system forming an approximately planar three-atom framework (Figure 1).[1−5] The double bond character acquired by the C−N bond increases its rotational barrier by more than 10 kcal/mol as compared to ordinary amines, for which roughly 4 kcal/mol is required to twist a C−N linkage.[6] Such an elevated energy barrier is largely responsible, for instance, for the conformational stability of proteins and enzymes through peptide bonds.[7−9]

Currently, a great deal of knowledge has been accumulated about the origin of the barrier and its response to the medium

(1) Stewart, W. E.; Siddall, T. H., III *Chem. Rev.* **1970**, *70*, 517−551.
(2) Wiberg, K. B.; Rablen, P. R.; Rush, D. J.; Keith, T. A. *J. Am. Chem. Soc.* **1995**, *117*, 4261−4270.
(3) Laidig, K. E.; Cameron, L. M. *J. Am. Chem. Soc.* **1996**, *118*, 1737−1742.
(4) Lauvergnat, D.; Hilberty, P. C. *J. Am. Chem. Soc.* **1997**, *119*, 9478−9482.
(5) Lim, K.-T.; Francl, M. M. *J. Phys. Chem.* **1987**, *91*, 2716−2721.

10.1021/jo061934u CCC: $37.00
Published on Web 02/17/2007

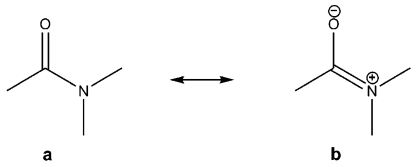

FIGURE 1. Resonance structures used to explain the barrier to C−N rotation in amides and correlated compounds.

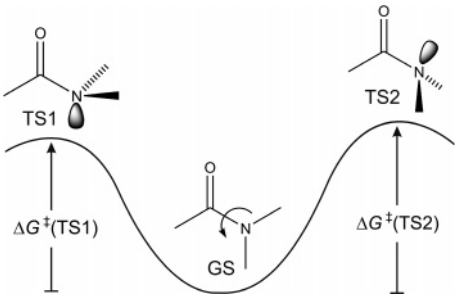

FIGURE 2. Transition states (**TS1** and **TS2**) generated by rotation over the central C−N bond of the planar ground state (**GS**).

for amides.[2−4,10−20] The comprehensive study of Wiberg et al.[2] demonstrated that the rotational barrier in amides increases with the solvent polarity and proton donor ability. For *N*,*N*-dimethylformamide and *N*,*N*-dimethylacetamide, variations of 4 and 2 kcal/mol, respectively, were observed when passing from the gas phase to a water solution. Such increases could be rationalized on the basis of the transition states for the process as follows. Rotation over the C−N bond breaks the conjugation and generates two transition states, **TS1** and **TS2** (Figure 2). Because the transition and ground states are expected to possess different dipole moments, the rotational barrier of amide-like systems should, in principle, vary with the solvent polarity, and this is indeed observed for amides.[2] Similar results were obtained for the corresponding sulfur derivatives, *N*,*N*-dimethylthioformamide and *N*,*N*-dimethylthioacetamide.[21] The rotational barriers are larger for the thioamides but still increase in polar

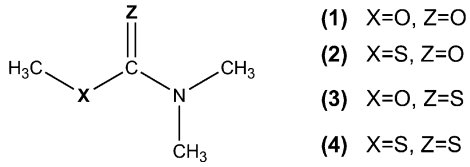

FIGURE 3. Structural formulas of the studied compounds.

solvents. Rablen et al.[22,23] performed related studies for *N*,*N*-dimethylaminoacrylonitrile and also for this compound they verified variations with the solvent.

Carbamates, −O−(C═O)−N<, bear the same amide framework and would be expected to have their rotational barrier changed by the solvent polarity. However, Cox and Lectka[8] demonstrated that the rotational barrier of carbamates is practically insensitive to the medium. Additionally, Rablen[24] calculated the dipole moments for the ground (**GS**) and transition states of methyl *N*,*N*-dimethylcarbamate and found an interesting situation because the differences between the dipoles of **GS** and the preferred transition state (**TS1**) were similar to those of amides. Even so, the calculations corroborated the experimental results of a small or vanishing solvent effect. The paradox was then solved by arguing that the solvent effect should be proportional to the **GS** dipole moment. This proposal was successful in explaining the distinct behavior of amides and carbamates because the dipole moment of the latter is about one-half of that of amides; this difference further increases if one assumes a quadratic behavior like the one of the Onsager theory.[25] Additionally, carbamates are poorer proton acceptors, which makes them less sensitive than amides to protic solvents.[24] Complementary studies by the present authors helped to confirm that the solvent insensitivity is a characteristic of the functional group carbamate, also clarifying the role of dipole moments and dipole moment variations in the rotation process.[26]

To get a better understanding of the rotational barrier in amide-like systems, it is necessary to extend the studies to a broader class of compounds. On the basis of this, we wished to see if sulfur substitution would maintain the carbamate behavior of no increase with the solvent polarity or proton donor ability. This was not the case, as described below. The inclusion of a third-row element was expected to affect the molecular structures in all of its aspects that are important to the rotational barrier behavior: polarizability, proton affinity, conjugation, and steric effects. Carbamates and thiocarbamates have been studied on several occasions regarding their rotational barrier, but unfortunately, the set of data is not enough to definitely establish the role of sulfur substitution on the solvent effect.[9,10,27−39] As we shall see, this is an issue where the combination of experimental measurements and theoretical calculations is of the most importance to achieve a clear understanding.

In this way, we selected four compounds, namely, methyl *N*,*N*-dimethylcarbamate (**1**), *S*-methyl *N*,*N*-dimethylthiocarbamate (**2**), *O*-methyl *N*,*N*-dimethylthiocarbamate (**3**), and methyl *N*,*N*-dimethyldithiocarbamate (**4**) (Figure 3). Each of them was prepared and subjected to experimental measurements by

(6) Benson, S. B. *Thermochemical Kinetics: Methods for Estimation of Thermochemical Data and Rate Parameters*, 2nd ed.; John Wiley & Sons: New York, 1976.
(7) Cox, C.; Lectka, T. *Acc. Chem. Res.* **2000**, *33*, 849−858.
(8) Cox, C.; Lectka, T. *J. Org. Chem.* **1998**, *63*, 2426−2427.
(9) Souza, W. F.; Kambe, N.; Sonoda, N. *J. Phys. Org. Chem.* **1996**, *9*, 179−186.
(10) Deetz, M. J.; Forbes, C. C.; Jonas, M.; Malerich, J. P.; Smith, B. D.; Wiest, O. *J. Org. Chem.* **2002**, *67*, 3949−3952.
(11) Duffy, E. M.; Severance, D. L.; Jorgensen, W. L. *J. Am. Chem. Soc.* **1992**, *114*, 7535−7542.
(12) Feigel, M.; Strassner, T. *J. Mol. Struct. (Theochem.)* **1993**, *283*, 33−48.
(13) Jackman, L. M.; Cotton, F. A. *Dynamic Nuclear Magnetic Resonance Spectroscopy*; Academic Press: New York, 1975.
(14) Vassilev, N. G.; Dimitrov, V. *J. Mol. Struct.* **1999**, *484*, 39−47.
(15) Wiberg, K. B.; Breneman, C. M. *J. Am. Chem. Soc.* **1992**, *114*, 831−840.
(16) Wiberg, K. B.; Hadad, C. M.; Rablen, P. R.; Cioslowski, J. *J. Am. Chem. Soc.* **1992**, *114*, 8644−8654.
(17) Wiberg, K. B.; Laidig, K. E. *J. Am. Chem. Soc.* **1997**, *119*, 5935.
(18) Wiberg, K. B.; Laidig, K. E. *J. Am. Chem. Soc.* **1987**, *109*, 5935−5943.
(19) Wiberg, K. B.; Rablen, P. R. *J. Am. Chem. Soc.* **1995**, *117*, 2201−2209.
(20) Wiberg, K. B.; Rablen, P. R. *J. Am. Chem. Soc.* **1993**, *115*, 9234−9242.
(21) Wiberg, K. B.; Rush, D. J. *J. Am. Chem. Soc.* **2001**, *123*, 2038−2046.
(22) Rablen, P. R.; Miller, D. A.; Bullock, V. R.; Hutchinson, P. H.; Gorman, J. A. *J. Am. Chem. Soc.* **1999**, *121*, 218−226.
(23) Rablen, P. R.; Pearlman, S. A.; Miller, D. A. *J. Am. Chem. Soc.* **1999**, *121*, 227−237.
(24) Rablen, P. R. *J. Org. Chem.* **2000**, *65*, 7930−7937.
(25) Onsager, L. *J. Am. Chem. Soc.* **1936**, *58*, 1486−1493.
(26) Basso, E. A.; Pontes, R. M. *J. Mol. Struct. (Theochem.)* **2002**, *594*, 199−206.

TABLE 1. Activation Parameters for Compounds 1−4 Determined through DNMR Total Line Shape Analysis Measurements[a]

	1			**2**		
	$\Delta H^{\ddagger}$	$\Delta S^{\ddagger}$	$\Delta G^{\ddagger}$	$\Delta H^{\ddagger}$	$\Delta S^{\ddagger}$	$\Delta G^{\ddagger}$
CCl_4	–	–	–	–	–	–
Bz-d_6	–	–	–	–	–	–
CS_2	10.8 ± 0.3	−15.0 ± 1.2	15.3 ± 0.5	12.5 ± 0.7	−5.4 ± 2.8	14.0 ± 1.1
CD_2Cl_2	10.4 ± 0.6	−16.6 ± 2.1	15.3 ± 0.9	14.7 ± 1.0	1.7 ± 4.1	14.2 ± 1.6
CD_3OD	14.2 ± 0.6	−3.1 ± 2.1	15.2 ± 0.9	12.6 ± 1.1	−6.7 ± 4.2	14.6 ± 1.6
CD_3CN	12.9 ± 1.4	−7.0 ± 5.4	15.0 ± 2.1	13.5 ± 0.7	−2.8 ± 2.7	14.3 ± 1.1
20% D_2O/CD_3OD	10.1 ± 0.8	−17.1 ± 2.9	15.2 ± 1.2	9.7 ± 0.3	−17.7 ± 1.2	14.9 ± 0.5
DMSO-d_6	–	–	–	–	–	–
D_2O	11.6 ± 1.0	−10.6 ± 3.4	14.8 ± 1.4	11.6 ± 0.5	−10.8 ± 1.7	14.8 ± 0.7
	3			**4**		
	$\Delta H^{\ddagger}$	$\Delta S^{\ddagger}$	$\Delta G^{\ddagger}$	$\Delta H^{\ddagger}$	$\Delta S^{\ddagger}$	$\Delta G^{\ddagger}$
CCl_4	17.4 ± 0.3	−0.2 ± 0.9	17.5 ± 0.4	13.8 ± 0.4	−2.7 ± 1.2	14.6 ± 0.5
Bz-d_6	19.9 ± 0.8	8.0 ± 2.5	17.6 ± 1.1	15.1 ± 0.2	0.3 ± 0.5	15.0 ± 0.2
CS_2	–	–	–	–	–	–
CD_2Cl_2	–	–	–	–	–	–
CD_3OD	–	–	–	14.2 ± 0.1	−3.1 ± 0.4	15.2 ± 0.2
CD_3CN	17.4 ± 0.3	−0.2 ± 0.9	17.5 ± 0.4	15.7 ± 0.1	0.4 ± 0.3	15.6 ± 0.1
20% D_2O/CD_3OD	–	–	–	14.8 ± 0.2	−2.5 ± 0.6	15.5 ± 0.3
DMSO-d_6	18.7 ± 0.3	2.7 ± 0.7	17.9 ± 0.3	16.0 ± 0.2	0.0 ± 0.5	16.0 ± 0.2
D_2O	–	–	–	12.7 ± 0.2	−10.8 ± 0.6	15.9 ± 0.3

[a] $\Delta H^{\ddagger}$ and $\Delta G^{\ddagger}$ in kcal/mol and $\Delta S^{\ddagger}$ in cal/K mol.

dynamic nuclear magnetic resonance (DNMR) in solvents of varied polarity and proton-donor ability. The theoretical study was composed of electronic structure routines (ab initio and DFT) together with molecular dynamics simulations.

Results and Discussion

NMR Measurements. The results of total line shape analysis (TLSA) for compounds **1**−**4** are presented in Table 1. Our main interest is in activation Gibbs energies ($\Delta G^{\ddagger}$), but before commenting on them, let us make a brief analysis of entropies and enthalpies of activation. There are some cases in which the rotational barrier can be thought of almost completely as an enthalpic phenomenon,[8] e.g., compound **4** in DMSO or compound **3** in CCl_4, whereas for most of them, it is indispensable to include the entropic contribution. With a few exceptions, the activation entropies ($\Delta S^{\ddagger}$) are negative, and we are tempted to imagine a more organized solvation shell for the transition states (**TS1** and **TS2**). However, as already reported for amides[2] and also verified in the calculations to be presented (Table 4), the entropies are still negative in the gas phase where no solvation structure can affect its values.

The probable reason for the negative entropy is the loss of one vibrational mode when going from **GS** to **TS**, once the C−N torsion becomes an imaginary frequency and no longer contributes to the thermodynamic properties of the system.[2] The few cases for which the entropy is positive can be understood in terms of complexation with solvent molecules. For instance, it is known[40] that aromatic solvents complex to the planar **GS** of amides due to the effect associated with resonance structure **b** (Figure 1), an effect that disappears in the **TS**s. Thus, for the cases where the activation entropy is positive, the ground states seem to be more organized with the solvent molecules overcoming the negative gas-phase entropy.

Consider now the activation Gibbs energies that are what we effectively call rotational barriers. The values for **1** in Table 1 agree with previous studies[8,24,26] for carbamates both in the barrier magnitude and in its response to the medium, i.e., the absence of a representative variation upon changing the solvent polarity or hydrogen-bonding ability. (The rotational barrier in water is actually 0.5 kcal/mol smaller than that in CS_2 suggesting a decrease in the rotational barrier; however, the variation is smaller than the experimental error and this hypothesis cannot be confirmed by these data only.) Compound **2** presents a rotational barrier about 1.0 kcal/mol smaller than that for **1** in the apolar solvent CS_2, but the values become essentially equal for both in water. Thus, experiments suggest an increase in the rotational barrier of **2**. There is a limitation in this conclusion imposed by the experimental errors. To overcome this problem, we also used $\Delta G^{\ddagger}$ values calculated through the coalescence temperature procedure.[1] The method consists of measuring the limiting separation of the absorption frequencies of the exchanging methyl groups together with the temperature at which the two signals coalesce. Limitations due to the solvent freezing or boiling, however, prevented us from obtaining suitable data for

(27) Valega, T. M. *J. Org. Chem.* **1966**, *31*, 1150−1153.
(28) Martin, M. L.; Marbon, F.; Trierweller, M. *J. Phys. Chem.* **1981**, *85*, 76−78.
(29) Smith, B. D.; Goodenough-Lashua, D. M.; D'Souza, C. J. E.; Norton, K. J.; Schmidt, L. M.; Tung, J. C. *Tetrahedron Lett.* **2004**, *45*, 2747−2749.
(30) Yamagami, C.; Takao, N.; Takeuchi, Y. *Aust. J. Chem.* **1986**, *39*, 457−463.
(31) Lemire, A. E.; Thompson, J. C. *Can. J. Chem.* **1970**, *48*, 824−829.
(32) Kost, D.; Kornberg, N. *Tetrahedron Lett.* **1978**, *35*, 3275−3276.
(33) Gayathri Devi, K. R.; Sathyanarayana, D. N.; Manogaran, S. *Spectrochim. Acta* **1981**, *37A*, 31−36.
(34) Julià, S.; Ginebreda, A.; Sala, P.; Sancho, M.; Annunziata, R. C. F. *Org. Magn. Reson.* **1983**, *21*, 573−575.
(35) Kornberg, N.; Kost, D. *J. Chem. Soc., Perkin Trans. 2* **1979**, 1661−1664.
(36) Schlottmann, B. U. *Tetrahedron Lett.* **1971**, 1221−1224.
(37) Lustig, E.; Benson, W. R.; Duy, N. *J. Org. Chem.* **1967**, *32*, 851−852.
(38) Kleinpeter, E.; Kretschemer, M.; Borsdorf, R.; Widera, R.; Mühlstädt, M. *J. Prakt. Chem.* **1980**, *322*, 793−797.
(39) Kleinpeter, E.; Widera, R.; Mühlstädt, M. *J. Prakt. Chem.* **1977**, *319*, 133−139.
(40) Wayland, B. B.; Drago, R. S.; Henneike, H. F. *J. Am. Chem. Soc.* **1966**, *88*, 2455.

TABLE 2. Rotational Barriers ($\Delta G^{\ddagger}$ in kcal/mol) for Compounds 1, 2, and 4 Determined through the Coalescence Temperature Method[a]

	1			2			4		
	T_c[b]	$\Delta\nu$[c]	$\Delta G^{\ddagger}$	T_c[b]	$\Delta\nu$[c]	$\Delta G^{\ddagger}$	T_c[b]	$\Delta\nu$[c]	$\Delta G^{\ddagger}$
CCl_4	–	–	–	–	–	–	31.5	35.1	15.2[d]
Bz-d_6	–	–	–	–	–	–	54.7	149.0	15.5
CS_2	21.6	10.9	15.4	−5.8	6.6	14.2	–	–	–
CD_2Cl_2	5.9	3.6	15.2	−14.6	2.1	14.3	–	–	–
CD_3OD	11.6	4.1	15.4	−1.0	4.0	14.7	43.5	42.4	15.7
CD_3CN	−1.0	1.8	15.1	−7.8	2.3	14.6	43.6	43.5	15.7
20% D_2O/CD_3OD	11.8	6.0	15.2[d]	13.7	8.2	15.1	49.1	40.5	16.0
DMSO-d_6	–	–	–	–	–	–	54.7	34.1	16.5
D_2O	10.8	3.0	15.5[d]	17.7	9.3	15.3[d]	61.1	38.3	16.7

[a] Experimental errors for $\Delta G^{\ddagger}$ are within ±0.2 kcal/mol. [b] Coalescence temperature in °C. [c] Difference in the absorption frequencies of the nonequivalent methyl protons, in Hz. [d] For these cases, it was not possible to attain a suitable $\Delta\nu$, so these values are less reliable as compared to the remaining ones.

compound **3**. For the remaining compounds, it was possible to measure the rotational barriers with this method (Table 2). The advantage of using the coalescence temperature comes from the fact that the experimental errors are in the vicinity of ±0.2 kcal/mol, which is better, for example, than the TLSA values for **2**. The rotational barrier of compound **1**, according to Table 2, agrees with those obtained through TLSA both in magnitude and in the absence of solvent effect. The entries in Table 2 also show an increase of ∼1.0 kcal/mol for **2**, and now this value lies well above the experimental error, confirming that the rotational barrier for compound **2** does experience an increase with the solvent polarity and maybe with hydrogen bonding also.

On passing from CCl_4 to water, the rotational barrier in compound **4** undergoes an increase of 1.3 kcal/mol according to TLSA (Table 1), which is a representative increase above the experimental errors. The same behavior can be noticed in Table 2, and thus it is possible to assert that the rotational barrier of compound **4** suffers a representative solvent effect. Wiberg and Rush[21] verified that the barriers in thioamides are greater than that of amides and so are the solvent effects. A similar behavior is observed here for thiocarbamates; i.e., the rotational barrier variations in carbamates, if any, could not be detected by the experiments so far performed, but sulfur substitution puts the variations in a measurable plateau, except for compound **3**. For this particular one, we could not acquire data in protic solvents due to an apparent sample decomposition. The compound initially formed a homogeneous solution but soon separated phases accompanied by the evolution of a white smoke. This indicates a very strong water−solute interaction compromising even the molecular stability; we did not go deeper into the reactivity of this compound as it is not the focus of the present study. In aprotic media, there are no representative variations for compound **3**.

To understand how the rotational barriers of these four compounds respond to the solvent medium, we performed theoretical calculations using electronic structure methods as well as liquid simulations by molecular dynamics, as described hereafter.

Rotational Barriers Determined through a Continuum Solvation Model. Amides and thioamides commonly adopt the conformation labeled as **GS1** in Figure 4.[14] That was also our starting point for the present compounds, but the outcome was somewhat different for the sulfur derivatives. Thus, it was necessary to conduct a conformational search prior to advancing with the theoretical studies. There are in principle four candidates for the ground-state conformation, labeled as **GS1**−**GS4** in Figure 4, and these were submitted to full geometry optimization and to frequency calculations (HF and B3LYP) to establish their stationary point nature. Both **1** and **2** exist in only one form from B3LYP as well as from HF, namely, **GS1**. Contrastingly, we found two conformations for **3** and **4**, and in these cases, the theoretical methods provide different results.

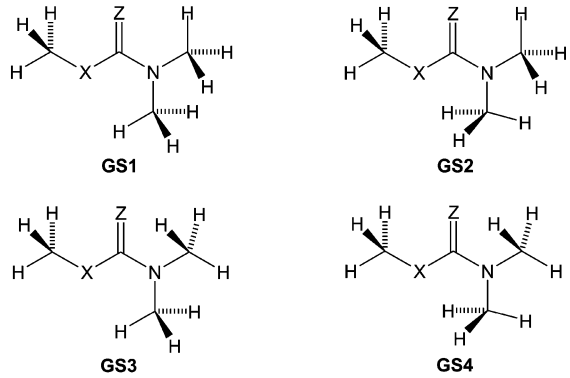

FIGURE 4. Possible conformations for the studied compounds.

Conformations **GS2** and **GS3** are stable at HF for **3**, with the two being almost isoenergetic (0.02 kcal/mol in favor of **GS2**), but for B3LYP, only **GS2** was obtained. A possible reason for this divergence is the differences in the structural parameters provided by each method. The C−H bond eclipsing the (C═S)−N bond in the *anti*-methyl group of **GS3** (Figure 4) is 2.197 Å from the oxygen atom (−O−) at HF, whereas at B3LYP, this distance is slightly smaller (2.188 Å) increasing the steric repulsion. Moreover, it is known that electron correlation methods tend to put more electron density on the molecular periphery relative to HF.[41] Together, both factors make **GS3** unstable at B3LYP.

In the case of **4**, conformations **GS2** and **GS4** are stable at B3LYP and only **GS4** exists with HF. A similar argument may be invoked here. The distance between the carbon in the *syn*-methyl group and the double-bonded sulfur atom is 2.973 Å at HF and 2.994 Å at B3LYP in **GS2**. Therefore, steric repulsion should be greater at HF making conformation **GS2** converge to **GS4**.

For the transition states **TS1** and **TS2**, we used structures like those depicted in Figure 2, both of them having only one imaginary frequency corresponding to the (C═Z)−N torsion which characterizes these structures as the correct first-order saddle points.

(41) Hadad, C. M.; Rablen, P. R.; Wiberg, K. B. *J. Org. Chem.* **1998**, *63*, 8668−8681.
(42) Lide, D. R. *CRC Handbook of Chemistry and Physics*, 77th ed.; CRC Press: Boca Raton, 1996.

TABLE 3. Gas-Phase Activation Parameters for Compounds 1−4 Calculated at the HF/6-311+G(2d,p) and B3LYP/6-311+G(2d,p) Levels of Theory[a]

	HF			B3LYP		
	$\Delta H^{\ddagger}$	$\Delta S^{\ddagger}$	$\Delta G^{\ddagger}$	$\Delta H^{\ddagger}$	$\Delta S^{\ddagger}$	$\Delta G^{\ddagger}$
1						
TS1	12.86	−7.08	14.97	13.86	−8.28	16.33
TS2	13.89	−6.71	15.89	14.77	−7.90	17.12
eff.[b]			14.86			16.19
2						
TS1	9.71	−6.53	11.66	11.66	−5.52	13.40
TS2	13.51	−5.90	15.29	14.82	−5.80	16.55
eff.[b]			11.66			13.40
3[c]						
TS1	15.16	−9.00	17.84	14.52	−9.21	17.27
TS2	16.14	−8.46	18.66	15.97	−8.86	18.61
eff.[b]			17.71			17.21
4[d]						
TS1	11.12	−11.56	14.56	11.45	−7.78	13.77
TS2	15.38	−10.59	18.53	15.54	−6.90	17.60
eff.[b]			14.56			13.77

[a] $\Delta H^{\ddagger}$ and $\Delta G^{\ddagger}$ in kcal/mol and $\Delta S^{\ddagger}$ in cal/K mol. [b] Effective barrier, incorporating the contribution of both transition states. [c] Conformation **GS2** was used. [d] Conformation **GS4** was used.

The stable conformations were then used to obtain vacuum rotational barriers (Table 3). As mentioned before, the gas-phase activation entropies are negative, a behavior that is maintained on passing to solutions for most cases as demonstrated by the experimental results. Nevertheless, gas-phase barriers must not be directly compared to experiments, as it is first necessary to include condensed-phase effects.

The solvation energy may be dissected into two components, namely, the bulk solvent polarity and specific solute−solvent interactions such as hydrogen bonding. The former can be directly handled by quantum methods, whereas specific interactions require the inclusion of statistical aspects of liquids, a task accomplished by classical-based protocols (Monte Carlo or molecular dynamics). Let us first consider the solvent polarity. For this purpose, we employed the isodensity polarizable continuum model (IPCM) as described in the Experimental Section.

The solution rotational barriers were obtained by simply adding to $\Delta G^{\ddagger}$ (from Table 3) the corresponding solvation energies from single-point calculations of the gas-phase structures (Table 4). The rotational barrier of **1** increases slightly when one passes from the gas phase to water (0.6 kcal/mol at HF and 0.8 kcal/mol at B3LYP). If we consider only those solvents for which measurements have been done, i.e., CS_2 and D_2O, the variation is only 0.2 kcal/mol with HF and 0.3 kcal/mol with B3LYP. These small variations agree with experiments. Although both methods agree with each other in the response to the solvent, the B3LYP values are about 2 kcal/mol above the experimental results (∼15 kcal/mol, Table 1).

Regarding compound **2**, the predicted solvent effect is 1.0 kcal/mol for both HF and B3LYP, which agrees with the experimental results. However, the calculated barriers are, on average, 1.0 kcal/mol below the experimental values at HF and about 1.0 kcal/mol above the experimental values at B3LYP. This result gives evidence that a further correction needs to be added to the calculated barriers.

When one passes from CCl_4 to DMSO, the rotational barrier for compound **3** varies by 0.8 kcal/mol at HF and by 0.7 kcal/mol at B3LYP. The experimental variation is 0.4 kcal/mol and stays within the experimental errors, so that it is not possible

TABLE 4. Rotational Barriers ($\Delta G^{\ddagger}$, in kcal/mol) for Compounds 1−4 Calculated at the HF/6-311+G(2d,p) and B3LYP/6-311+G(2d,p) Levels of Theory with Solvation Effects Included through the IPCM Method[a]

		TS1		TS1		eff.[b]	
		HF	B3LYP	HF	B3LYP	HF	B3LYP
				1			
ϵ	1.00	14.97	16.33	15.89	17.12	14.9	16.2
	2.23	15.41	16.81	16.03	17.41	15.2	16.6
	2.61	15.47	16.88	16.04	17.44	15.3	16.7
	32.61	15.84	17.29	16.03	17.59	15.5	17.0
	35.69	15.84	17.30	16.03	17.59	15.5	17.0
	46.83	15.85	17.30	16.03	17.59	15.5	17.0
	78.36	15.86	17.32	16.02	17.60	15.5	17.0
				2			
ϵ	1.00	11.66	13.40	15.29	16.55	11.7	13.4
	2.23	12.56	14.60	15.45	17.84	12.6	14.6
	2.61	12.70	14.75	15.47	17.88	12.7	14.8
	32.61	13.70	15.72	15.51	18.08	13.7	15.7
	35.69	13.70	15.73	15.51	18.08	13.7	15.7
	46.83	13.73	15.75	15.51	18.09	13.7	15.7
	78.36	13.76	15.78	15.51	18.09	13.7	15.8
				3[c]			
ϵ	1.00	17.84	17.27	18.66	18.61	17.7	17.2
	2.23	19.17	18.03	19.06	18.70	18.7	17.9
	2.61	19.37	18.17	19.14	18.73	18.8	18.0
	32.61	20.76	19.04	19.59	18.90	19.5	18.6
	35.69	20.77	19.04	19.59	18.90	19.5	18.6
	46.83	20.80	19.06	19.60	19.91	19.5	18.6
	78.36	20.84	19.09	19.61	18.91	19.5	18.6
				4[d]			
ϵ	1.00	14.56	13.77	18.53	17.60	14.6	13.8
	2.23	15.41	14.31	19.65	18.38	15.4	14.3
	2.61	15.54	14.40	19.80	18.50	15.5	14.4
	32.61	16.55	15.06	20.73	19.11	16.6	15.1
	35.69	16.56	15.06	20.74	19.11	16.6	15.1
	46.83	16.58	15.08	20.76	19.13	16.6	15.1
	78.36	16.62	15.10	20.78	19.14	16.6	15.1

[a] Dielectric constants, corrected to 25 °C, correspond to a vacuum, carbon tetrachloride, carbon disulfide, methanol, acetonitrile, dimethyl sulfoxide, and water.[42] [b] Effective barrier, incorporating the contribution of both transition states. [c] The conformation **GS2** was used. [d] The conformation **GS4** was used.

to ensure the observation of such an effect. What is most probable is that weak solute−solvent complexation effects mask the variation. This interpretation is supported by the measured entropy values. To see this, let us remember that the gas-phase theoretical activation entropies are negative (Table 3), whereas the experimental ones are positive or very close to zero for **3**. These results suggest that some kind of ordered state is broken on passing from the ground to the transition state, like a solute−solvent complex. Concerning the rotational barrier magnitude, neither HF nor B3LYP furnishes satisfactory results using only IPCM.

In the case of compound **4**, when one goes from CCl_4 to H_2O, the rotational barrier varies by 1.2 kcal/mol at HF and by 0.8 kcal/mol at B3LYP, in agreement with experiments. The HF barriers are somewhat above the experimental ones, and those calculated by B3LYP lie, on average, below the DNMR measurements.

To summarize, although the IPCM model is able to reproduce the solvent effect to some extent, it is still necessary to include explicit solute−solvent interactions. Among these interactions are those of very strong impacts on the solute properties, i.e., hydrogen bonds, and those that are more common among highly polarizable solvents, such as CS_2 or DMSO, which correspond to somewhat weaker, less geometrically restricted interactions.

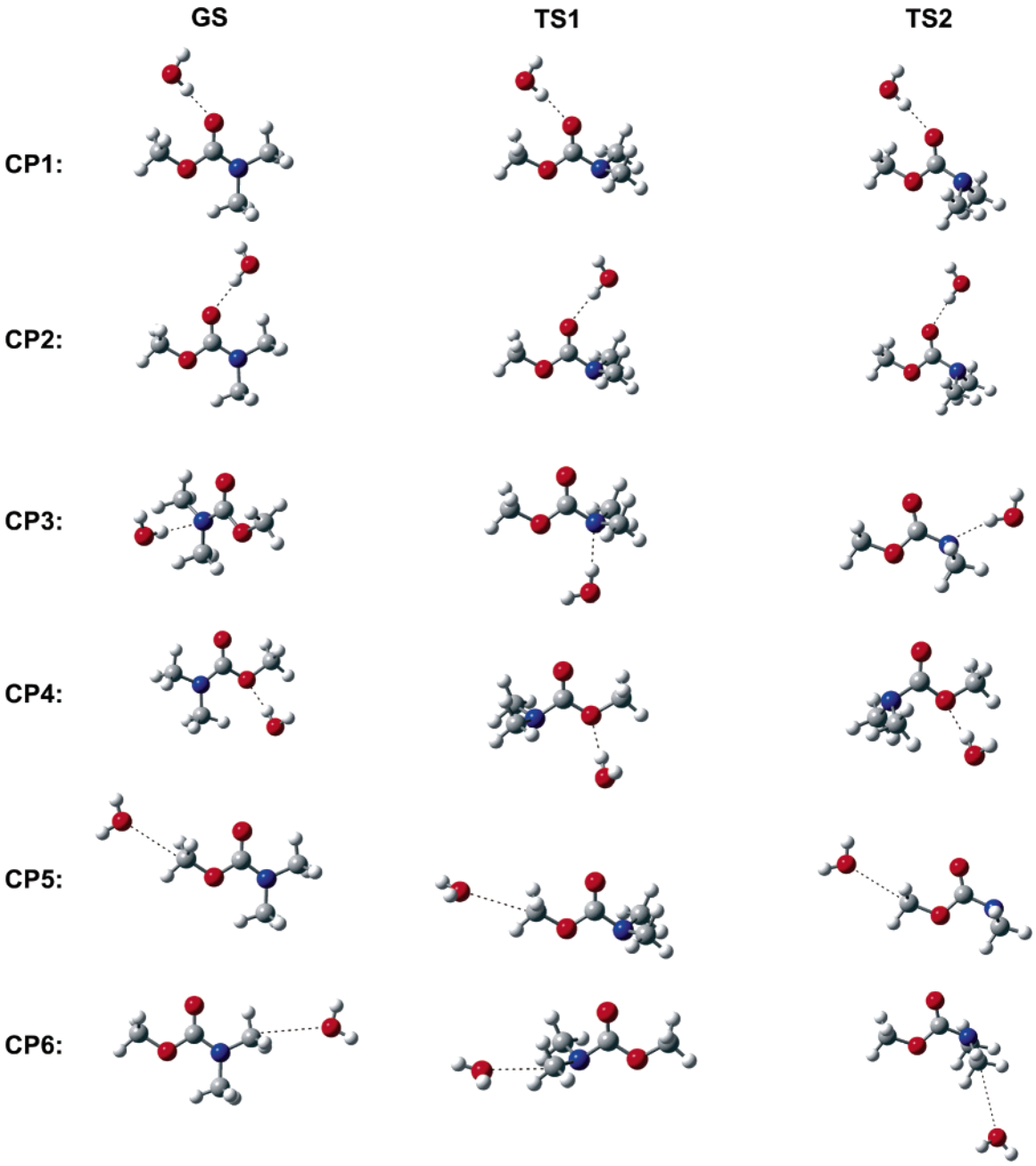

FIGURE 5. Water complexes used in the force-field parametrization of compounds **1**−**4**.

For the present study, we will treat only hydrogen bonding through molecular dynamics simulations. Whether HF or B3LYP provides better rotational barriers can be judged only after including these interactions.

Force-Field Parametrization. Liquid simulations require the specification of solute−solvent potential interaction functions. These are defined by Coulomb (electron charges) and Lennard−Jones (van der Waals) parameters adjusted for every atom or atom groups.[11] Unfortunately, there were no such parameters for the present compounds; those reported for amides did not furnish satisfactory results when extended to carbamates and thiocarbamates in our tests. Therefore, it was necessary to calibrate the potential interaction functions before running the liquid simulations. To accomplish this task, we followed a procedure similar to that used by Jorgensen et al.[11] We first built complexes of the solute with a water molecule placed in strategic positions and then calculated the complex energy at the B3LYP/6-31+G(d,p) level (Figure 5). Through this calculation, the solute was kept at the B3LYP/6-311+G(2d,p) geometry while the water molecule was fixed with its TIP4P parameters (r(O−H) = 0.9752 Å, ∠(H−O−H) = 104.52°);[43] only the distance between the two molecules was optimized. The partially optimized geometries were then used to perform a counterpoise correction for the basis set superposition error (BSSE) and to obtain interaction energies, ΔE_{int}. There are three atomic quantities composing Coulomb and Lennard−Jones potentials, namely, the electron charge, q, and the two Lennard−Jones

(43) Jorgensen, W. L.; Chandrasekhar, J.; Madura, J. D. *J. Chem. Phys.* **1983**, *79*, 926−935.

TABLE 5. Solute−Water Complexation Energies (in kcal/mol) Calculated at the B3LYP/6-31+G(d,p) Level of Theory (DFT) and through the Fitted Force Field (FF)[a]

	1		2		3		4	
	DFT	FF	DFT	FF	DFT	FF	DFT	FF
				GS				
CP1	−6.21	−6.32	−4.87	−4.43	−2.79	−2.93	−2.77	−2.68
CP2	−5.91	−5.98	−5.51	−5.89	−2.46	−2.60	−2.42	−2.57
CP3	−1.20	−1.32	−1.07	−0.80	−1.23	−1.42	−0.68	−0.56
CP4	−2.24	−2.37	−2.01	−1.74	−0.51	−1.22	−2.30	−2.30
CP5	−0.79	−0.65	−0.24	−0.84	−0.85	−0.57	−0.28	−0.42
CP6	−0.83	−0.80	−0.97	−1.22	−1.02	−0.63	−1.15	−1.11
rms[b]		*0.11*		*0.39*		*0.37*		*0.11*
				TS1				
CP1	−5.38	−5.28	−4.64	−4.39	−2.26	−2.16	−2.20	−2.11
CP2	−4.96	−4.90	−4.49	−4.66	−1.58	−1.67	−1.54	−1.77
CP3	−5.91	−5.93	−4.47	−4.61	−5.13	−5.10	−3.99	−3.95
CP4	−1.62	−1.56	−1.35	−1.30	−1.05	−0.50	−1.03	−0.91
CP5	−1.32	−1.54	−0.57	−1.05	−1.21	−1.22	−0.72	−0.86
CP6	−0.54	−0.98	−0.30	−1.01	−0.36	−0.50	−0.21	−0.73
rms[b]		*0.21*		*0.38*		*0.24*		*0.25*
				TS2				
CP1	−5.36	−5.53	−4.46	−4.34	−2.32	−2.32	−2.29	−2.17
CP2	−4.44	−4.16	−3.92	−4.05	−1.28	−1.29	−1.25	−1.32
CP3	−5.88	−5.55	−5.45	−5.32	−5.68	−5.66	−5.49	−5.07
CP4	−1.04	−0.93	−1.73	−1.28	−0.42	−0.46	−1.36	−1.26
CP5	−1.51	−1.24	−0.74	−1.16	−1.52	−1.66	−0.69	−1.14
CP6	−0.55	−1.11	−0.56	−1.30	−0.39	−0.54	−0.48	−1.02
rms[b]		*0.32*		*0.40*		*0.09*		*0.34*

[a] Complexes CP1−CP6 are defined in Figure 5. [b] Root mean square deviations (in kcal/mol).

parameters accounting for van der Waals forces, ϵ and σ. These parameters determine the interaction energy according to the following equation:

$$\Delta E_{\text{int}} = \sum_i \sum_j \{q_i q_j e^2/r_{ij} + 4\epsilon_{ij}[(\sigma_{ij}/r_{ij})^{12} - (\sigma_{ij}/r_{ij})^6]\} \quad (1)$$

in which

$$\epsilon_{ij} = \sqrt{\epsilon_i \epsilon_j}, \quad \sigma_{ij} = \sqrt{\sigma_i \sigma_j}$$

Throughout the force-field calculations, we used a model with each methyl group being described as a single atom, giving a seven-point representation of the solute molecular structure. A further simplification was to describe the two CH_3's attached to N by the same atom type. Lennard−Jones parameters (ϵ, σ) were taken from similar compounds,[11,44−47] and only the atomic charges were varied to reproduce DFT interaction energies. Table 5 presents the results of the adjusted force field together with the DFT values. The complete set of fitted electron charges along with the Lennard−Jones parameters used are included as Supporting Information. The agreement between DFT and force-field values was satisfactory in most cases, so they can be considered as appropriate to be used in the liquid simulations.

Radial Distribution Functions. After obtaining the force-field parameters, we performed molecular dynamics calculations on water solutions of the four compounds. Because each compound has three species (**GS**, **TS1**, and **TS2**), there is a total of 12 simulations, as described in the Experimental Section. The coordinates stored during MD runs were used to construct radial distribution functions (rdf) for each pair of solute−solvent atoms. These functions are constructed such that in structured portions of the liquid, like those close to the solute, its value differs from the unit with a maximum indicating a likely region for finding solvent molecules. In the bulk liquid, far from the solute, rdf's approach unit values and no region is more likely to contain solvent molecules than others. Hydrogen bonding can be identified by a sharp peak at about 2 Å (O···H rdf). The rdf's for compounds **1**−**4** are presented in Figure 6.

Solvation peaks are clearly observed in the **GS** of **1** for both C═O···O(water) and C═O···H(water) rdf's. The distance between the maxima of the two rdf's is 0.95 Å, very close to the O−H bond length in the TIP4P model, showing that there is an efficient complexation between the solute and water molecules at the carbonyl oxygen. On the other hand, there is no indication of hydrogen bonding at the nitrogen of **GS**, as expected, following from the sp^2 hybridization of that atom. The situation is a little different in the **TSs**. Here, beyond the bonding at the carbonyl oxygen, water molecules also complex at the nitrogen which is now sp^3 and has a lone pair available to donate electron density. These results suggest, even before we quantify the effects, that the rotational barrier of **1** decreases as a consequence of hydrogen bonding because the **TSs** have two binding sites compared to only one in the **GS**.

The rdf's of compound **2** resemble those for **1** in their qualitative aspects. However, the N···H and N···O peaks in the **TSs** are, relative to **1**, less intense. As we are going to see, this causes the effect of hydrogen bonding in **2** to be the opposite of that for **1**; i.e., the rotational barrier will increase from complexation to protic solvents.

Another aspect that can be explained by rdf's is the negative activation entropies in the protic solvents of Table 1. The measured $\Delta S^{\ddagger}$ values in D_2O are about twice the calculated gas-phase values for **1** and **2**, which suggest that in the corresponding transition states water molecules might be more organized around the solute compared to the ground state. Looking at the rdf's, the reason becomes clear, for the **GSs** of **1** and **2** have only one protonation site compared to two in the **TS**, confirming the more ordered state of the latter. A similar effect could be invoked to explain the negative entropy in D_2O/CD_3OD. The effect in this case, however, is more intense, but without detailed molecular dynamic data in methanol, we cannot unequivocally describe this subtle behavior.

Although for **1** and **2** we observe hydrogen bonding at the carbonyl oxygen of **GS**, compounds **3** and **4**, contrastingly, present no signal of complexation at the corresponding double-bonded sulfur atoms. On the other hand, both transition states engage in hydrogen bonding to water, although in a smaller fashion in the case of **TS1**. Because only the transition states are stabilized by complexation, we expect the rotational barriers of **3** and **4** to experience a decrease in protic solvents.

Rotational Barriers with the Inclusion of Hydrogen Bonding. The following step is to quantify the effect of hydrogen bonding on the rotational barriers. The solvation peaks previously identified can be integrated out to the first minimum, furnishing, in this way, the average number of water molecules engaging in a water−solute complex. Table 6 presents these results. Complexation energies were obtained by simply multiplying the average number of water molecules in the solvation shell by the corresponding energies in Table 5. For instance,

(44) Jorgensen, W. L. *J. Phys. Chem.* **1986**, *90*, 1276−1284.
(45) Jorgensen, W. L. *J. Phys. Chem.* **1986**, *90*, 6379−6388.
(46) Jorgensen, W. L.; Madura, J. D.; Swenson, C. J. *J. Am. Chem. Soc.* **1984**, *106*, 6638−6646.
(47) Jorgensen, W. L.; Swenson, C. J. *J. Am. Chem. Soc.* **1985**, *107*, 569−578.

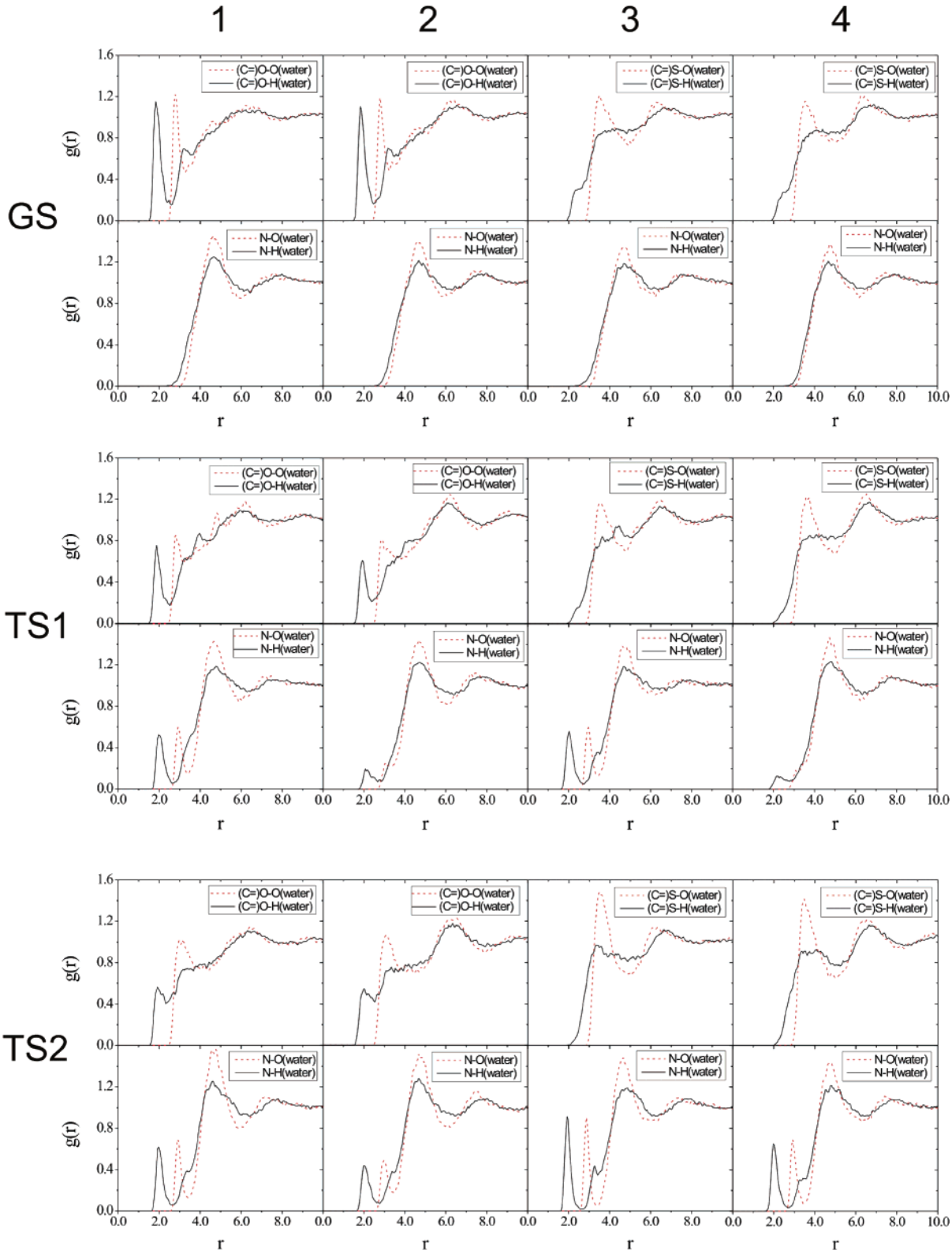

FIGURE 6. Radial distribution functions for compounds **1**−**4**.

when one water molecule binds the **GS** of **1** at the carbonyl, the system gains 6.06 kcal/mol of stability (average between **CP1** and **CP2**, Table 5); however, 1.7 water molecules, on average, surround **GS** according to the rdf's (Table 6), and thus the overall stabilization becomes −10.21 kcal/mol. The last column of Table 6 lists the contribution of hydrogen bonding to the rotational barriers.

The smallest effect occurs for **1** corresponding to a decrease in the barrier. Decreases are observed also for **3** and **4** with higher intensity than those in **1**. Only for **2**, hydrogen bonding

TABLE 6. Analysis of Radial Distribution Functions for Compounds 1−4

	C═Z		N		total		
species	coord.[a]	ΔE^b	coord.[a]	ΔE^b	coord.[c]	ΔE^d	$\Delta\Delta E^e$
			Methyl *N*,*N*-Dimethylcarbamate (**1**)				
GS	1.69 (*2.53*)	−10.21	–[f]	–[f]	1.69	−10.21	
TS1	1.08 (*2.43*)	−5.60	0.89 (*2.63*)	−5.28	1.97	−10.88	−0.67
TS2	1.12 (*2.38*)	−5.50	0.92 (*2.63*)	−5.41	2.04	−10.91	−0.70
			S-Methyl *N*,*N*-Dimethylthiocarbamate (**2**)				
GS	1.56 (*2.48*)	−8.09	–[f]	–[f]	1.56	−8.09	
TS1	0.93 (*2.38*)	−4.24	0.44 (*2.68*)	−1.97	1.37	−6.21	+1.88
TS2	0.71 (*2.18*)	−2.95	0.84 (*2.68*)	−4.58	1.55	−7.53	+0.56
			O-Methyl *N*,*N*-Dimethylthiocarbamate (**3**)				
GS	–[f]	–[f]	–[f]	–[f]			
TS1	–[f]	–[f]	0.92 (*2.73*)	−4.72	0.92	−4.72	−4.72
TS2	–[f]	–[f]	1.01 (*2.68*)	−5.71	1.01	−5.71	−5.71
			Methyl *N*,*N*-Dimethyldithiocarbamate (**4**)				
GS	–[f]	–[f]	–[f]	–[f]			
TS1	–[f]	–[f]	0.36 (*2.73*)	−1.44	0.36	−1.44	−1.44
TS2	–[f]	–[f]	0.93 (*2.68*)	−5.10	0.93	−5.10	−5.10

[a] Number of water molecules coordinated to solute obtained by integration of the (C═)Z···H(water) rdf; cutoff radii are presented in parentheses and in Å. [b] Solute−water complexation energies (in kcal/mol) calculated on the basis of the data of Table 5 and the above coordination numbers. [c] Total number of coordinated water molecules obtained by summing up the contributions of (C═)Z and N. [d] Total complexation energy (in kcal/mol) obtained by summing up the contributions of (C═)Z and N. [e] Total contribution of hydrogen bonding (in kcal/mol) to the rotational barriers. [f] No solvation shell observed for these rdf's.

TABLE 7. Rotational Barriers in Water (in kcal/mol) for Compounds 1−4 Calculated Using the Combination IPCM + MD

	TS1		TS2		eff.[a]		
	B3LYP	HF	B3LYP	HF	B3LYP	HF	exptl
1	17.00	15.19	17.25	15.32	16.7	14.8	14.8 ± 1.4
2	17.99	15.64	19.08	16.07	17.9	15.4	14.8 ± 0.7
3	14.39	16.12	13.24	13.90	13.2	13.9	–
4	13.66	15.18	14.00	15.68	13.4	15.0	15.9 ± 0.3

[a] Effective barriers, including the contribution of both transition states.

contributes to an increase in the rotational barrier. These results contrast with those of amides which have their barriers raised in protic solvents,[19] and as far as we are aware, there is no previous report of a negative solvent effect on the rotational barrier of an amide-like system.

Table 7 lists the final rotational barriers calculated by the IPCM + MD combination. These values were obtained by adding the effect of hydrogen bonding just mentioned to the data of Table 4. The B3LYP values now diverge greatly from experimental measurements, whereas HF presents a very satisfactory agreement. Before including both sets of effects—solvent polarity and specific interactions—it was not possible to correctly judge the performance of each method. It can be seen now that the inclusion of electron correlation through DFT is not advantageous for the calculation of rotational barriers. Actually, this was noted before by Wiberg et al.[2] for gas-phase calculations. Additionally, Jasien et al.[48] found that electron correlation is not essential for calculating rotational barriers in amides; their analyses were based on MP2 calculations. We have conducted an earlier study[26] on the rotational barrier of carbamates using DFT-B3LYP in which good agreement was obtained between calculated and experimental values. In that occasion, however, we did not use the thermodynamic quantities but rather total energies corrected to zero-point vibrations.

Let us now analyze the reasons for the above-mentioned behaviors. As we said while commenting on the rdf's for compound **1**, the transition states engage in hydrogen bonding in two places, at the carbonyl and at the nitrogen, and the ground state accepts bonding only at the carbonyl. Integration of the corresponding rdf's (Table 6) shows that these two interactions in the **TS**s are responsible for the rotational barrier diminution. This behavior is readily explained by the resonance model because the nitrogen passes from sp^2 to sp^3 hybridization on going from **GS** to **TS** and becomes a good proton acceptor (Figure 2).

A similar pattern is observed for compound **2**, but in this case, the hydrogen-bonding strength produces a different outcome. The nitrogen here is not as good of a proton acceptor as it is for **1** in the **TS**, so despite the **TS**s having two protonation sites, the **GS** experiences the greater stabilization. It is seen from Table 6 that the preferred transition state for **2**, **TS1**, forms about one-half of the hydrogen bonds of the corresponding **TS** of **1**, 0.44 vs 0.89. Indeed, Mulliken analysis gives −0.326 e for the nitrogen in the **TS1** of **1**, compared to −0.058 e for the nitrogen in the **TS1** of **2** (at HF/6-311+G(2d,p)). Moreover, the large sulfur atom of **2** makes the approach of water molecules at **TS1** difficult and also contributes to lowering its proton-acceptor ability.

Consider now compounds **3** and **4**. The rotational barrier decreases for both as a consequence of hydrogen bonding, and the effect here is substantially larger than in **1**. For these compounds, as mentioned before, there is no hydrogen bonding with the double-bonded sulfur atom in either **GS** or **TS**, so that the complexation at the nitrogen of **TS** causes the barrier to decrease. Similarly to what we mentioned above for the **TS1** of **2**, the additional sulfur atom of **4** repels the approach of water molecules to the nitrogen region, making hydrogen bonding in the **TS1** of **4** less effective. When these effects are added to the IPCM results, the calculated rotational barrier of **4** is found to be in satisfactory agreement with the experimental value. Unfortunately, there is no experimental data for compound **3** in water. Given the good performance of IPCM + MD for the other compounds, we should expect a rotational barrier for **3** in water in the vicinity of 14 kcal/mol, about 4 kcal/mol lower than the value in DMSO (Table 4).

Dipole Moments. As a final step, let us consider the connection between dipole moments and the response to the solvent polarity. Because HF and B3LYP agree with each other about the variations in the IPCM results, we think it is advisable to analyze dipole moments calculated through both methods, and these are presented in Table 8. Ground-state dipole moments for **1** and **2** are very similar, as also are the variations when passing to **TS1**. Therefore, similar solvation effects should be expected for these species, but this does not happen because the data in Table 4 clearly show a far more pronounced effect in **2**, about 2.0 kcal/mol compared to only 0.4 kcal/mol in **1** (vacuum to water). Neither **GS** dipole moments nor variations in dipole moments can alone account for the differences between these compounds.

Now, let us look at the rotation **GS** → **TS1** for compounds **3** and **4**. In this case, both μ and $\Delta\mu$ are greater for **3**, the compound for which the solvent effect is also larger (+3.00 kcal/mol compared to +2.06 kcal/mol on going from $\epsilon = 1.00$ to $\epsilon = 78.36$, Table 4). We see, therefore, that considering the

(48) Jasien, P. G.; Stevens, W. J.; Krauss, M. *J. Mol. Struct. (Theochem.)* **1986**, *139*, 197−206.

TABLE 8. Calculated Dipole Moments and Dipole Moment Differences (in D) for Compounds 1−4[a,b]

	μ (GS)		Δm (TS1)[c]		Δm (TS2)[c]	
	HF	B3LYP	HF	B3LYP	HF	B3LYP
			1			
vacuum	2.56	2.48	−1.65	−1.62	+0.45	+0.18
water	3.61	3.67	−2.21	−2.30	+0.44	+0.23
			2			
vacuum	2.25	2.31	−1.66	−1.59	−0.21	−0.19
water	3.63	3.80	−2.28	−2.24	−0.16	−0.29
			3			
vacuum	4.28	3.68	−2.52	−2.29	−0.72	−0.71
water	6.04	5.32	−3.82	−3.73	−1.29	−1.32
			4			
vacuum	3.74	3.31	−2.55	−2.09	−1.12	−0.89
water	5.34	4.75	−3.19	−2.54	−1.77	−1.32

[a] **GS2** for **3** and **GS4** for **4**. [b] Basis set 6-311+G(2d,p). [c] Variation on going from **GS** to **TS** [$\Delta\mu = \mu(\mathbf{TS}) - \mu(\mathbf{GS})$].

quantities μ or $\Delta\mu$, as we did above, may or may not lead to the correct result for the solvent effect trend. To put things in a more systematic scheme, we can use the approximation introduced by Onsager,[25] writing the solvation energy of a given molecule in terms of its dipole moment, μ, and of a spherical cavity of radius, a_o:

$$\Delta G_{solv} = -\frac{\epsilon - 1}{2\epsilon + 1}\frac{\mu^2}{a_o^3} \quad (2)$$

If the dipoles of **GS** and **TS** differ by $\Delta\mu$, the **TS** dipole moment can be written as $\mu_{\mathbf{TS}} = \mu_{\mathbf{GS}} + \Delta\mu$. The solvation energy for **TS** then becomes

$$\Delta G_{solv}^{\mathbf{TS}} = -\phi(\epsilon,a_o)\mu_{\mathbf{GS}}^2 - 2\phi(\epsilon,a_o)\mu_{\mathbf{GS}}\Delta\mu - \phi(\epsilon,a_o)(\Delta\mu)^2 \quad (3)$$

where

$$\phi(\epsilon,a_o) = \frac{\epsilon - 1}{2\epsilon + 1}\frac{1}{a_o^3}$$

The solvent effect for the process **GS** → **TS** is simply defined by

$$\Delta\Delta G_{solv} = \Delta G_{solv}^{\mathbf{TS}} - \Delta G_{solv}^{\mathbf{GS}} \quad (4)$$

Under the assumption that the molecular radius does not vary too much from **GS** to **TS**, we finally arrive at

$$\Delta\Delta G_{solv} = -2\phi(\epsilon,a_o)\mu_{\mathbf{GS}}\Delta\mu - \phi(\epsilon,a_o)(\Delta\mu)^2 \quad (5)$$

The first thing to be noted when analyzing solvation effects in terms of dipole moments (μ) or dipole moment variations ($\Delta\mu$) is that both quantities must be considered simultaneously, and eq 5 gives us an idea of how μ and $\Delta\mu$ relate to the solvent effect on rotational barriers. If we have two compounds with a similar μ, they will behave as distinctly as the differences in their $\Delta\mu$. If, instead, the $\Delta\mu$ are similar, then the relative behavior will be dictated by $\mu_{\mathbf{GS}}$. The contributions of each member of eq 5 are listed in Table 9.

The simple approximations introduced above work well for compounds **1**, **3**, and **4**, as can be seen by comparing the values of the dipole moment model to those calculated with IPCM, but it fails for **2** probably due to the importance of higher multipole moments or cavity approximations. The correct trends in the solvent effect are reproduced with dipole moments from the gas-phase structures, but only after using the dipoles from a previous solvated structure (IPCM) can we obtain a reasonable estimate of the effect on the rotational barrier. The $\Delta\mu$ values are all negative for the rotation **GS** → **TS1** implying that the first term of eq 5 will raise the barrier for compounds **1**−**4**. The largest effect occurs for **3**, which has the largest μ and $\Delta\mu$. The smallest effect is observed for **1**, for which both μ and $\Delta\mu$ assume their lowest values.

TABLE 9. Partition of Energy Terms Contributing to the Solvent Effect According to the Spherical Cavity Approximation (a_o in Å and the Remaining Values in kcal/mol)

a_o (TS1)	μ calcd in	$-2\phi(\epsilon,a_o)\mu_{\mathbf{GS}}\Delta\mu$	$-\phi(\epsilon,a_o)(\Delta\mu)^2$	total dipole	total IPCM
			1		
4.09	vacuum	0.87	−0.28	+0.59	+0.89
	water	1.65	−0.50	+1.15	
			2		
4.11	vacuum	0.76	−0.28	+0.48	+2.10
	water	1.68	−0.53	+1.15	
			3		
4.36	vacuum	1.84	−0.54	+1.30	+3.00
	water	3.93	−1.24	+2.69	
			4		
4.33	vacuum	1.66	−0.57	+1.10	+2.06
	water	2.97	−0.89	+2.08	

Conclusions

Rotational barriers in amide-like systems are generally affected by solvation. Nevertheless, the effect can sometimes be too small to detect by experimental procedures, as is the case with carbamates. For carbamates, *O*-alkyl thiocarbamates, and dithiocarbamates, protic solvents decrease the barrier through hydrogen bonding. *S*-Alkyl thiocarbamates, however, have their barrier raised in protic media. Carbamates experience only a little decrease in their rotational barrier due to hydrogen bonding because the two protonation sites at the transition states, the carbonyl and the nitrogen, are roughly balanced by hydrogen bonding at the carbonyl of the ground state. The inability of the sulfur atom to form hydrogen bonds is responsible for the large decrease observed for compounds **3** and **4** in water solutions because in these cases only the transition states will be stabilized by hydrogen bonding.

Combining the continuum solvation method IPCM with molecular dynamics proved to be a suitable protocol for analyzing solvation effects in solvents that engage in hydrogen bonding with the solute. Rotational barriers for carbamate congeners are better calculated through Hartree−Fock than with the B3LYP method. Even so, on the basis of the final calculated barriers, B3LYP furnished satisfactory results when used to obtain solute−solvent complexation energies. Solute−solvent complexation energies calculated at the B3LYP/6-311+G(2d,p) level, statistically corrected by radial distribution functions, can be used to quantify hydrogen-bonding effects on the rotational barriers. The final calculated results seem to slightly overestimate the experimental effects but are still reliable in reproducing the observed barriers and their response to the medium.

Replacing oxygen with a sulfur atom can cause two effects, depending on where the replacement takes place. In particular, the sulfur atom in **2** hinders the approach of a water molecule

to the nitrogen of **TS1** and causes this transition state to lose some of the stabilization energy it could gain from hydrogen bonding. This contributes to increasing the barrier corresponding to **TS1**, which is the preferred transition state of **2**.

Three of the four compounds studied behave in a way explainable by dipole moments and dipole moment variations. Compound **2** is the exception and is a good example for not extrapolating conclusions before a careful evaluation of a wide range of structural systems.

Experimental Section

Syntheses. Compounds were obtained following the procedures described by Yoder et al.[4949] Methyl *N*,*N*-dimethylcarbamate (**1**) was prepared by the reaction of sodium methoxide with *N*,*N*-dimethylcarbamoyl chloride in tetrahydrofuran (THF) (bp 128 °C/∼760 Torr, lit.[49] 130−132 °C/∼760 Torr). ^{1}H NMR (300 MHz, $CDCl_3$) δ: 3.69 (3H, s); 2.91 (6H, s).[49,50]

S-Methyl *N*,*N*-dimethylthiocarbamate (**2**) was prepared by the reaction of sodium thiomethoxide with *N*,*N*-dimethylthiocarbamoyl chloride in tetrahydrofuran. Sodium thiomethoxide was obtained from the isothiouronium salt procedure[51] by bubbling methyl mercaptan in a mixture of THF and Na^o (bp 54 °C/>6 Torr, lit.[49] 184 °C/∼760 Torr). ^{1}H NMR (300 MHz, $CDCl_3$) δ: 2.96 (6H, s); 2.29 (3H, s).

O-Methyl *N*,*N*-dimethylthiocarbamate (**3**) was prepared by the reaction of sodium methoxide with *N*,*N*-dimethylthiocarbamoyl chloride in THF (bp 76 °C/>7 Torr, lit.[49] 87−92 °C/12 Torr). ^{1}H NMR (300 MHz, $CDCl_3$) δ: 4.02 (3H, s); 3.74 (3H, s); 3.12 (3H, s).

Methyl *N*,*N*-dimethyldithiocarbamate (**4**) was prepared by the reaction of *N*,*N*-dimethylamine with methyl iodide and carbon disulfide (mp 43−44 °C, lit.[49] 45−47 °C). ^{1}H NMR (300 MHz, $CDCl_3$) δ: 3.57 (3H, s); 3.38 (3H, s); 2.65 (3H, s).

NMR Measurements. A 300 MHz spectrometer was used to acquire ^{1}H spectra. Samples were prepared by placing 15 μL (for liquid) or 20 mg (for solid) of the compound in 0.7 mL of the appropriate solvent in 5-mm o.d. NMR tubes. In the case of carbon disulfide, acetone-d_6 was used as an external reference. Typical conditions were a sweep width of 2500 Hz, a pulse length of 6.7 μs, 16 scans, and 1 s for the delay time. 32 K of data points were used for acquisition with further zero filling to 64 K. Line broadening was not applied. Deuterated solvents were obtained commercially and used as received, and CS_2 was distilled and stored under molecular sieves prior to use. The variable-temperature probe was calibrated against vacuum-sealed methanol (−70 to 15 °C) and ethylene glycol (20−80 °C) standards.[52,53] Total line shape analyses (TLSA) were accomplished using the WINDNMR[54] software.

Computational Details. Electronic structure calculations were conducted using the GAUSSIAN 98[55] package of programs. Geometries were optimized using the restricted Hartree−Fock (RHF) method as well as the hybrid B3LYP density functional, both with the 6-311+G(2d,p) basis set. A subsequent frequency calculation characterized the stationary points (one imaginary frequency for transition states and zero for ground states), from which we also obtained thermodynamics quantities.[56] The effect of solvent polarity was included through the isodensity polarizable continuum model (IPCM)[57] at the HF/6-311+G(2d,p) and B3LYP/6-311+G(2d,p) levels by single-point calculations over the corresponding optimized structures. The IPCM solvation model had been used in related studies and proved to be suitable for representing the energy variations due to bulk solvent polarity in rotational barriers.[2,23,24] In this model, the solute is placed in a cavity defined by an isosurface of the total electron density (typically 0.0004 e/bohr^2). The model not only treats dipole moments but also is equivalent to going to an infinite order in a multipole expansion.[57]

Molecular dynamics simulations of water solutions were carried out with the TINKER[58] package of programs. The TIP4P model[43] was employed to describe the water molecules, whereas for solutes, it was necessary to conduct a force-field parametrization (as detailed in Results and Discussion). Rigid models were used. Simulations were performed in the NVT ensemble with 296 water molecules plus the corresponding solute in a pre-equilibrated box with dimensions 20.80 × 20.80 × 20.80 Å. After equilibrating the box at 298 K for 20 ps, production periods lasted 300 ps with a temperature couple parameter of 0.3 ps and a time step of 0.001 ps.

Acknowledgment. The authors are thankful to Centro Nacional de Processamento de Alto Desempenho (CENAPAD-SP) for the computer facilities and to Fundação de Amparo à Pesquisa do Estado de São Paulo (FAPESP) for financial support. We also give thanks to Coordenação de Aperfeiçoamento de Pessoal de Nível Superior (CAPES) for a scholarship to R. M. Pontes and to Conselho Nacional de Pesquisa (CNPq) for a fellowship to E. A. Basso.

Supporting Information Available: ^{1}H NMR spectra and *Z*-matrices for the optimized structures and force-field parameters for MD simulations. This material is available free of charge via the Internet at http://pubs.acs.org.

JO061934U

(49) Yoder, H. C.; Komoriya, A.; Kochanowski, J. E.; Suydam, F. H. *J. Am. Chem. Soc*. **1971**, *93*, 6515−6518.

(50) Basso, E. A.; Oliveira, P. R. O.; Caetano, J.; Schuquel, I. T. A. *J. Braz. Chem. Soc*. **2001**, *12*, 215−222.

(51) Frank, R. L.; Smith, P. V. *J. Am. Chem. Soc*. **1946**, *68*, 2103−2104.

(52) Greet, A. L. v. *Anal. Chem.* **1970**, *42*, 679.

(53) Raidford, D. S.; Fisk, C. L.; Becker, E. D. *Anal. Chem*. **1979**, *51*, 2050.

(54) Reich, H. J. *J. Chem. Educ*. Software 3D2.

(55) Frisch, M. J.; Trucks, G. W.; Schlegel, H. B.; Scuseria, G. E.; Robb, M. A.; Cheeseman, J. R.; Zakrzewski, V. G.; Montgomery, J. A., Jr.; Stratmann, R. E.; Burant, J. C.; Dapprich, S.; Millam, J. M.; Daniels, A. D.; Kudin, K. N.; Strain, M. C.; Farkas, O.; Tomasi, J.; Barone, V.; Cossi, M.; Cammi, R.; Mennucci, B.; Pomelli, C.; Adamo, C.; Clifford, S.; Ochterski, J.; Petersson, G. A.; Ayala, P. Y.; Cui, Q.; Morokuma, K.; Malick, D. K.; Rabuck, A. D.; Raghavachari, K.; Foresman, J. B.; Cioslowski, J.; Ortiz, J. V.; Stefanov, B. B.; Liu, G.; Liashenko, A.; Piskorz, P.; Komaromi, I.; Gomperts, R.; Martin, R. L.; Fox, D. J.; Keith, T.; Al-Laham, M. A.; Peng, C. Y.; Nanayakkara, A.; Gonzalez, C.; Challacombe, M.; Gill, P. M. W.; Johnson, B. G.; Chen, W.; Wong, M. W.; Andres, J. L.; Head-Gordon, M.; Replogle, E. S.; Pople, J. A. *Gaussian 98*, revision A.11.2; Gaussian, Inc.: Pittsburgh, PA, 1998.

(56) Foresman, J. B.; Frisch, Æ. *Exploring Chemistry with Electronic Structure Methods*, 2nd ed.; Gaussian, Inc.: Pittsburgh, 1996.

(57) Foresman, J. B.; Keith, T. A.; Wiberg, K. B.; Snoonian, J.; Frish, M. J. *J. Phys. Chem*. **1996**, *100*, 16098−16104.

(58) Ponder, J. W. *TINKER: Software tools for molecular design*; version 4.1; Washington University School of Medicine: St. Louis, 2003.